Korean J. Chem. Eng., 38(1), 104-113 (2021)
DOI: 10.1007/s11814-020-0650-y

pISSN: 0256-1115
eISSN: 1975-7220

Effect of halloysite nanotubes incorporation on morphology and CO_2/CH_4 separation performance of Pebax-based membranes

Seyed Mohammad Ali Ahmadi, Toraj Mohammadi†, and Navid Azizi

Center of Excellence for Membrane Science and Technology, School of Chemical, Petroleum and Gas Engineering, Iran University of Science and Technology (IUST), Narmak, Tehran, Iran
(*Received 3 February 2020 • Revised 24 May 2020 • Accepted 2 August 2020*)

Abstract−Mixed-matrix gas separation membranes were prepared by embedding various content of halloysite nanotubes (HNTs) (0, 0.5, 1, 1.5, and 2 wt%) within poly (ether-block-amide) matrix. XRD, FT-IR, TGA, and SEM analyses were conducted to study crystal structure, chemical bonds changes, thermal resistance, and cross-sectional morphology of the resultant membranes, respectively. Permeability values of pure CH_4 and CO_2 gases through the synthesized neat and mixed-matrix membranes (MMMs) were experimentally determined at constant temperature (25 °C) and several pressures (4, 6, 8, and 10 bar). The obtained results exhibited improved CO_2 permeability of the MMMs comparing with the pristine Pebax membrane. As an example, at a pressure of 4 bar, raising the incorporated HNTs loading from 0 to 2 wt% enhanced the permeability of CO_2 from 76.50 to 101.23 Barrer.

Keywords: CO_2/CH_4 Separation, Pebax-1657-based Mixed-matrix Membrane, Halloysite Nanotubes

INTRODUCTION

The presence of carbon dioxide (CO_2) in natural gas, of which methane (CH_4) is its principal component, can reduce its heating value, as well as corrode gas pipelines and other equipment when it reacts with water and carbonic acid (H_2CO_3) is produced. Hence, removal of CO_2 and other acid gases like H_2S, RSH, and SO_2 from natural gas is the most significant concern in the gas industry. During the last few decades, various industrial approaches have been utilized for CO_2/CH_4 separation, which are mainly processes based on adsorption, chemical and physical absorption, and membrane separation [1]. Membrane separation processes have several benefits over traditional separation techniques, such as lower capital and operating expenses, higher energy saving, higher operational flexibility, safer for the environment, less required space, and more lightweight, which make them attractive candidates for high-efficiency separation applications [2]. However, gas separation membranes are still of their deficiencies like low processing capacity, plasticization, and physical aging [3]; therefore, finding solutions to overcome these problems is a great challenge for membrane research. Choosing suitable membrane materials is a critical factor in synthesis of highly efficient membranes. Regarding the importance of material selection for fabricating a polymeric membrane applied to CO_2/CH_4 separation, it is inevitable that the chosen polymer has more remarkable affinity to polar CO_2 molecules than non-polar ones (CH_4). Moreover, it should possess suitable thermal, chemical, and mechanical resistance to tolerate various operating conditions.

Among the most commonly used polymers, poly (ether-block-amide), commercially called Pebax®, fulfils the mentioned requirements, and consequently can be regarded as a promising polymer for the gas sweetening process [4,5]. This polymer is a group of elastomers having a total structure of $(PA\text{-}PE)_n$, is composed of hard and soft segments with short blocks and linear chains. The former is polyamide (PA) and the latter is polyether (PE). At a typical ambient temperature, the hard block exhibits a glassy state, whereas the soft one is rubbery; therefore, the ratio of PA to PE blocks determines the Pebax hardness [6,7]. Since the PE segment chains are highly mobile, it can be responsible for penetrant permeability through the Pebax-based membrane, while the crystalline PA block is a dense and impermeable part of Pebax. As polar gases show good affinity to the polar groups of Pebax, they are expected to permeate more than non-polar ones through the Pebax membranes [8-10]. Notably, the PA segment length influences directly on the melting point of the Pebax, and due to the immiscibility of PE and PA segments, the Pebax is of bi-phase morphology. Here, Pebax with a grade of 1657, comprising 60 wt% of PE and 40 wt% of PA, was chosen as the polymer for the membrane preparation [8-14]. Some specific characteristics of the Pebax-1657 are listed in Table 1.

Permeability-selectivity trade-off limitations among polymeric membranes used in gas separations are almost their major difficulty Numerous investigators have endeavored to pass the upper-bound suggested by Robeson using various physical or chemical amend-

Table 1. Pebax-1657 physical features

Mechanical characteristic	Value
Density	1.14 g·cm^{-3}
Melting point	204 °C
Water adsorption at 23 °C for 24 h remaining in water	120 wt%
Stress at break	32 MPa
Glass transition temperature	−56 °C

†To whom correspondence should be addressed.
E-mail: torajmohammadi@iust.ac.ir

ments on the pristine membranes [15-17]. Low cost, processability, and intrinsic transport properties of polymeric membranes can be combined with particular features of inorganic materials, donating extra characteristics to the prepared membranes such as the ability of gas separation even at high temperatures and pressures when they are incorporated into the polymer base materials. In fact, the introduction of inorganic nanomaterials to the polymeric matrices due to their specific chemical and physical properties influences on gas molecules transport through the resulting membranes, and consequently, the membrane selectivity values can be improved [1,18-22]. Such membranes, which are termed mixed-matrix membranes (MMMs), also cause the thermal and chemical stability of the neat membranes to improve [23,24].

Recently, Azizi et al. [25] surveyed the CO_2/CH_4 separation performance of Pebax-based MMMs filled with TiO_2. The experimental results revealed that the MMM composed of 8 wt% of the TiO_2 exhibited optimum efficiency based on CO_2/CH_4 selectivity and CO_2 permeability. Xu et al. [26] studied gas (CO_2, N_2 and CH_4) transport characteristics of Pebax-based MMMs incorporated with ZIF-8 nanofillers. Their permeation test results indicated that enhancing nanoparticle loading up to 18 wt% caused permeability of all the gases to grow considerably. Accordingly, CO_2/CH_4 and CO_2/N_2 selectivity values of the membranes increased. In another study, Zhao et al. [27] prepared MMMs with Pebax-1657 and SAPO-34 nanoparticles and showed that with enhancing the nanoparticle loading, permeabilities of N_2, CH_4, H_2 and CO_2 were improved, whereas CO_2/H_2, CO_2/N_2 and CO_2/CH_4 selectivity values did not change considerably [21,28-32]. Molecular sieves like various zeolites, carbon nanotubes, as well as aluminosilicate minerals show desirable gas permeability, selectivity or both than the polymer-based membranes as they are embedded with the polymer matrix. Halloysite is a naturally occurring clay that mostly consists of multi-walled nanotubular-shaped crystals and has been reported as a new interesting filler to reinforce polymers. Halloysite nanotubes (HNTs) were eventuated from the wrapping of the clay layers around themselves to create hollow cylinders under suitable geological conditions [33]. These nanoparticles have high specific surface area, high availability, low cost and significantly high potency for adsorption of CO_2 molecules. However, less attention has been devoted to them. Therefore, they can be taken into consideration as satisfactory nanofillers for preparing high-performance MMMs in gas separation. There are few studies on incorporating HNTs into polymeric matrices for gas separation applications.

Ismail et al. [34] studied the facilitated transport influence of Ag^+ ion-exchanged HNTs as a nanofiller on gas separation efficiency of polyetherimide (PEI)-based MMMs. They showed that by increasing the HNTs loading within the polymer matrix, the permeability of CH_4 and CO_2 gases and selectivity of the membranes experienced ascending and ascending-descending trends, respectively. In another study by Murali et al. [33], polyaniline in situ modified halloysite nanotubes (PANi-HNTs) were embedded into polysulfone (PSF) and gas (CO_2, O_2, CH_4, and N_2) permeation characteristics of the synthesized MMMs were investigated. Their results showed that permeance values of all the gases grew with enhancing the PANi-HNTs content in PSF matrix. Besides, by augmenting the HNTs loading up to 1 wt%, CO_2/CH_4, and CO_2/N_2 selectivity was improved; however, it was observed that at the higher loadings, the selectivity dropped. Hashemifard et al. [35] studied gas transport characteristics of prepared asymmetric PEI-based MMMs incorporated with pure and modified HNTs. They experimentally observed that with augmenting the modified-HNTs loading from 0 to 1 wt%, CO_2 permeability rose, while CO_2/CH_4 selectivity exhibited an ascending-descending trend. Based on CO_2 permeability and CO_2/CH_4 selectivity, the MMM loaded with 0.5 wt% of modified-HNTs was selected as the optimum membrane.

Although numerous MMMs have been so far prepared for CO_2/CH_4 separation, the introduction of new nanomaterials into polymer matrices may result in fabrication of high-performance membranes; therefore, attempts for preparation of novel MMMs are still being continued. To the best knowledge of the authors, this was the first try of improving Pebax-1657 with HNTs to prepare MMMs for the CO_2/CH_4 separation. The HNTs loading effects on the membranes structure and their separation performance were investigated.

MATERIALS AND METHODS

1. Materials

HNTs ($Al_2Si_2O_5(OH)_4 \cdot 2H_2O$) with length of 1-3 μm, internal and external diameters of 30 and 70 nm, respectively, specific surface area of 64 $m^2 \cdot g^{-1}$ was supplied from Sigma Aldrich Co. Pebax-1657 as a basic membrane material was purchased from Arkema Inc. Dimethylformamide (DMF) as a solvent for the membrane fabrication and pure gases (CO_2 and CH_4) for gas permeation tests were provided from Merck and Farafan Gas Company, respectively.

2. Membrane Preparation

Before the membrane fabrication process was started, the Pebax granules and the HNTs were kept in a vacuum oven, which was adjusted at a temperature of 70 °C for about 6 h to eliminate any adsorbed moisture. To fabricate the pristine membrane, a specific quantity of the polymer granules (2.5 wt%) was combined with the solvent (DMF). Afterward, the mixture vessel was put in an oil bath at 115 °C and agitated for at least 6 h magnetically. After the perfect dissolution of the Pebax granules in the DMF, the obtained solution was first passed through a steel filter and then poured into a glassy Petri-dish of radius 3.5 cm. The cast sample was then kept for 14 h in an oven at 50 °C. After that, the resultant membrane was gently parted from the Petri-dish, and until usage put in a desiccator [36,37].

For the MMMs fabrication, specific amounts of the HNTs (0.5, 1, 1.5, and 2 wt% of the Pebax mass) were added into the solvent. Then, the mixtures were placed under sonication for 30 min and left in an oil bath at 120 °C. The polymer granules were then added into the mixtures during three-time intervals in order to prime the HNTs. This process facilitates better interaction between the Pebax and HNTs, which finally results in superior dispersion of the HNTs in the mixture. The same drying technique applied to synthesize the neat membrane was obeyed after agitating the mixture for about 6 h magnetically. Based on the HNTs loading within the polymer matrix, the prepared membranes were named M_0, M_0.5, M_1, M_1.5, and M_2. Additionally, a digital micrometer was employed to measure the thicknesses of the fabricated membranes.

3. Membrane Characterization

3-1. Scanning Electron Microscopy (SEM)

Scanning electron microscopy (TESCAN-VEGA II, Czech Republic) was employed for studying the morphology of the resulting membranes. The samples were fractured in liquid nitrogen, then mounted on stainless steel stands and before taking cross-sectional images, coated with gold via a sputter coater.

3-2. X-Ray Diffraction (XRD)

A JEOL, JDX-8030 diffractometer was used to conduct XRD analysis of the membranes, identifying the crystal structure of the Pebax-1657 and intermolecular distances among its intersegment chains influenced by the nanofillers. The diffraction angle (2θ) changed from 5 to 75° using Cu Kα as the radiation source.

3-3. Fourier Transform Infrared (FT-IR)

A Shimadzu 8400S spectrometer was employed for recording FT-IR spectra of the HNTs and the dried membrane samples. One mg of each sample being well ground along with a specific amount of KBr (100 mg) was moved to a plate before recording the IR spectra at 400-4,000 cm^{-1} wavenumber range.

3-4. Thermal Gravimetric Analysis (TGA)

For the study of the synthesized membranes' thermal stability, STA 504 thermal gravimetric analyzer (BÄHR-Thermoanalyse GmbH) was applied. About 10 mg of each sample was placed in a sample maintainer and heated up to 600 °C at 10 °C·min^{-1} rate in air atmosphere.

4. Gas Permeation Test

Gas permeation tests were carried out over a pressure range of 4-10 bar at 25 °C to evaluate the separation efficiency of the fabricated membranes. A traditional fixed-pressure gas experiment setup was used to measure CO_2 and CH_4 permeability for the flat sheet membrane samples, as depicted in Fig. 1 [38-40]. A flat circular membrane sample of 2.5 cm effective radius was put in a module comprising two detachable stainless steel sections joined by two rubber O-rings where the membrane sample is embedded between them to make a pressure seal system available and avoid any gas leakage possibility from the cell, as well. For conducting the gas permeation tests, the pure gases were exposed to the membrane cell at pressures of 4, 6, 8, and 10 bar, being set via two pressure regulators, while the permeate side was linked to the atmosphere. The feed temperature was adjusted at 25 °C for all the tests by putting the membrane module in an oven.

Employing a typical bubble flow-meter, the permeated gas flow rate was measured. All the permeation data were reported after about 3 h when a steady-state situation was obtained. After that, the permeability coefficient of the gases was determined by the below equation [41]:

$$P_i = 10^{10} \times \frac{273.15}{76} \times \frac{p}{T} \times \frac{Q_i \times l}{\Delta p \times A} \quad (1)$$

where P_i, l, Q_i, T, p, Δp, and A are permeability of the gas i (Barrer), the membrane thickness (cm), the flow rate of the gas i ($cm^3 \cdot s^{-1}$), the feed side temperature (K), the permeate side pressure (cmHg), which was atmospheric pressure in the permeation experiments, the difference between the feed and permeated gas pressures (cmHg), and the membrane area (cm^2), respectively. In this study, for reducing experimental error, each permeation experiment was carried out three times and the mean permeability coefficients along with their standard deviations were presented.

The ideal selectivity of the synthesized membranes was obtained using the specified pure gas permeability (P_{CO_2} and P_{CH_4}) as follows [42]:

$$\alpha_{CO_2/CH_4} = \frac{P_{CO_2}}{P_{CH_4}} \quad (2)$$

RESULTS AND DISCUSSION

1. Characterization

1-1. SEM

The morphology of membranes strongly influences the gas permeation rates; therefore, their morphology study using SEM analysis is necessary. SEM analysis can be performed to investigate the

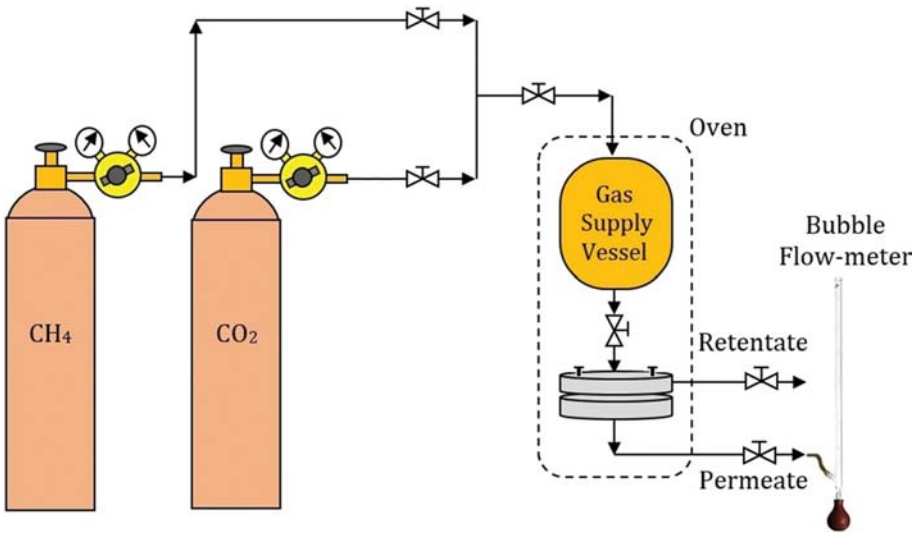

Fig. 1. Schematic representation of the membrane module and gas permeation setup.

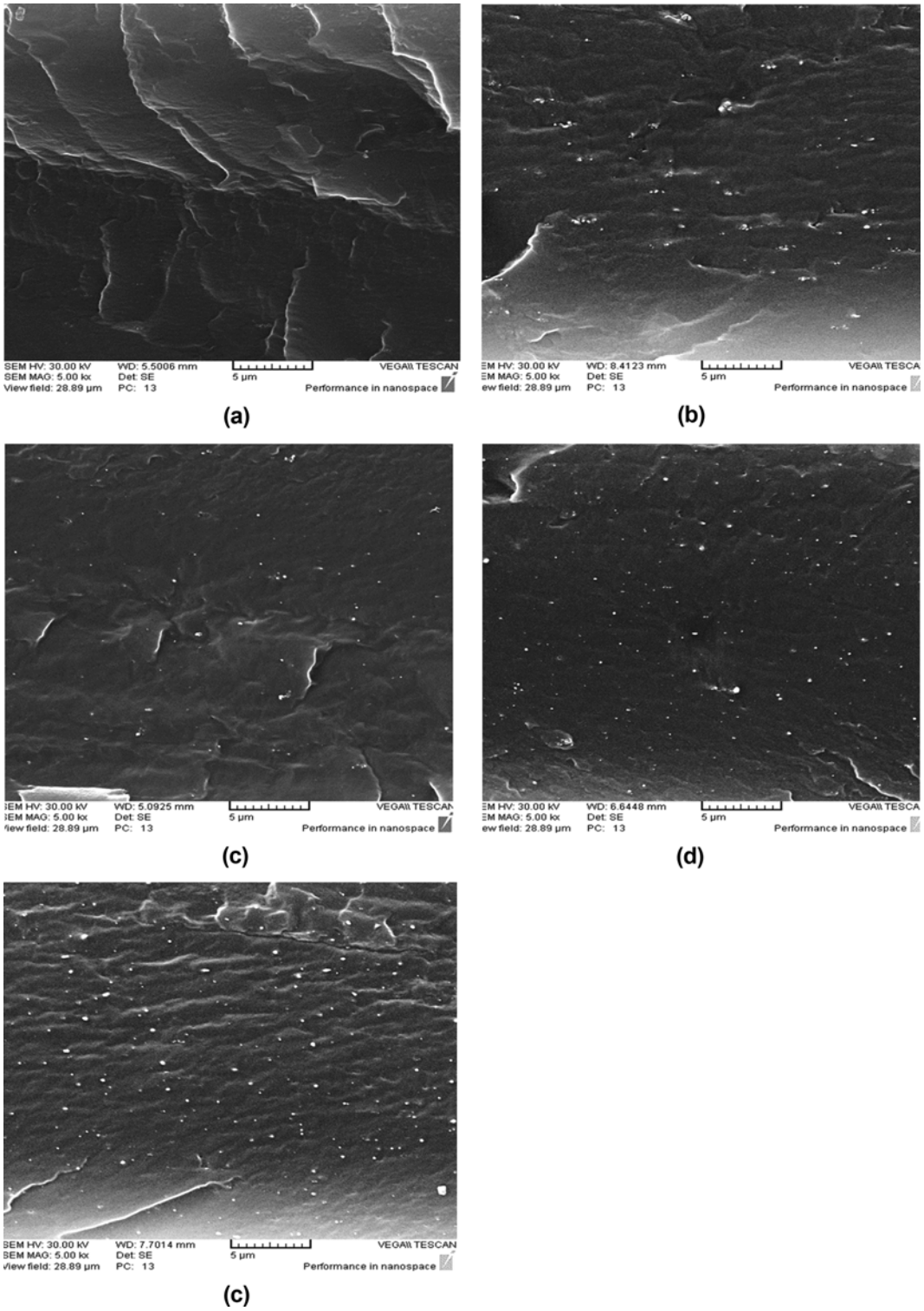

Fig. 2. Cross-sectional SEM pictures of the resulting membranes: (a) M_0, (b) M_0.5, (c) M_1, (d) M_1.5, and (e) M_2.

presence, dispersion, aggregation, and phase separation of the nanofillers. SEM images taken from cross-sections of fabricated MMMs embedded with different amounts of HNTs are displayed in Fig. 2. As depicted in Fig. 2(a), the pristine membrane is of a completely dense structure having no particular deficiency. As seen in Fig. 2(b), (c), and (d), the uniform spread of the HNTs in the Pebax matrix without the formation of significant cavities at the Pebax-HNTs interface is detected. Fine dispersal process of the HNTs in the Pebax matrix, along with desirable adhesion of the HNTs to the polymer are the main reasons for the lack of creation of voids (cavity formation) around the nanotubes. The SEM photos include light and nearly dark regions, which are indicative of the nano-

tubes and the continuous polymeric phase, respectively. These images reveal the nanometer size of the well-dispersed HNTs within the polymeric matrix of the Pebax. As observed in Fig. 2(e), the M_2 membrane composed of 2 wt% of HNTs possesses approximately uniform distribution of the nanotubes. However, the nanotubes tend to be gently agglomerated in the Pebax matrix when their loading exceeds 2 wt% of HNTs. The main reason why the HNTs tend to be aggregated and sedimented in the polymer matrix is the highly attractive energy between the nanotubes, as well as the considerable distinction of surface energies between the nanotubes and the polymer [40,43]. Hence, these energies should be decreased and balanced in order to obtain excellent dispersion of the HNTs in the Pebax matrix. In this study, for suitable distribution of the HNTs in the polymer matrix, a strong ultrasonic probe was added; therefore, the HNTs agglomeration in the polymer matrix was ignorable. It is noteworthy that the membrane thickness was measured by 50-60 μm.

1-2. XRD

Study of the crystalline structure of the prepared membranes is also vital for analyzing gas permeability and selectivity data resulting from the experiments. One of the most commonly used approaches for the investigation of membrane crystallinity is XRD analysis [44]. XRD pattern of the pristine membrane (M_0) in comparison to those of the prepared MMMs is presented in Fig. 3. The crystalline or amorphous nature of a polymer affects its diffraction peak intensity and position. Poly (ether-block-amide) polymers are of semi-crystalline structure having broad and sharp peaks ascribed to their PE and PA crystalline areas, respectively. Fig. 3 displays that the synthesized M_0 membrane possesses the mentioned intensified peak at 23.84° of 2θ and the weak peak at 2θ= 16.84°. Overall, the embedment of nanofillers within a membrane matrix can vary the resulting MMMs crystallinity degree [28,45]. As shown in Fig. 3, the augment of the HNTs into the Pebax structure resulted in the reduced membrane crystallinity. This can probably be as a result of the decrement of interchain hydrogen bonding and cohesive energy among PA segments via HNTs incorporation. Additionally, the locations of the peaks change to lower 2θ, which can enhance the d-spacing (d) values regarding Bragg's equation ($n\lambda=2d\sin\theta$) [46,47]. A combination of these alterations in the polymer structure increases the fractional free volume (FFV) of the prepared MMMs and, as a result, improves gas permeability values [48,49]. D-spacing is the extent of molecular distance among the polymer chains. The bigger the d-spacing value, the higher the gas molecules transport tendency [50]. The higher content of HNTs (2 wt%) into the polymer matrix results in more change in the prepared MMM d-spacing and crystallinity (Fig. 3). Consequently, it is expected that the MMM loaded with the highest HNTs content (M_2) renders the highest gas diffusivity and permeability coefficients. The obtained gas permeation data confirm this claim.

1-3. FT-IR

To confirm the successful HNTs inclusion in Pebax-1657 matrix, FT-IR analysis for the prepared membranes (M_0, M_0.5, M_1, M_1.5, and M_2) was carried out as shown in Fig. 4. For the M_0 membrane, symmetric vibration of the ether (C-O-C) functional group in the PE block can be observed via a peak at 1,101 cm^{-1}. The detected peaks at 1,641 and 1,728 cm^{-1} were related to the carbonyl (C=O) group vibration of H-N-C=O and O-C=O in the PA segment, respectively. Additionally, the observed peak at 3,238 cm^{-1} is representative of the vibration of N-H group in the PA segment. The characteristic peak at 2,866 cm^{-1} exhibited the existence of C-H aliphatic group [42,48,51].

Nearly, most peaks corresponding to the pristine membrane functional groups are seen with some variations in the MMMs spectra. For example, as seen in Fig. 4, the carbonyl and N-H groups in the PA segments of the MMMs shift to the higher wavenumbers. These changes can be a sign of the inter-chain hydrogen bonding disruption among the PA segments. Accordingly, it can be inferred that the crystallinity of the MMMs decreases as the HNTs loading in the polymer matrix increases. Another difference between the FT-IR spectra of the MMMs and that of the neat membrane is the existence of new peaks, which can be ascribed to the HNTs characteristic peaks. In Fig. 4, the spectrum of the HNTs shows peaks which correspond to deformation of Si-O-Si at 470 cm^{-1},

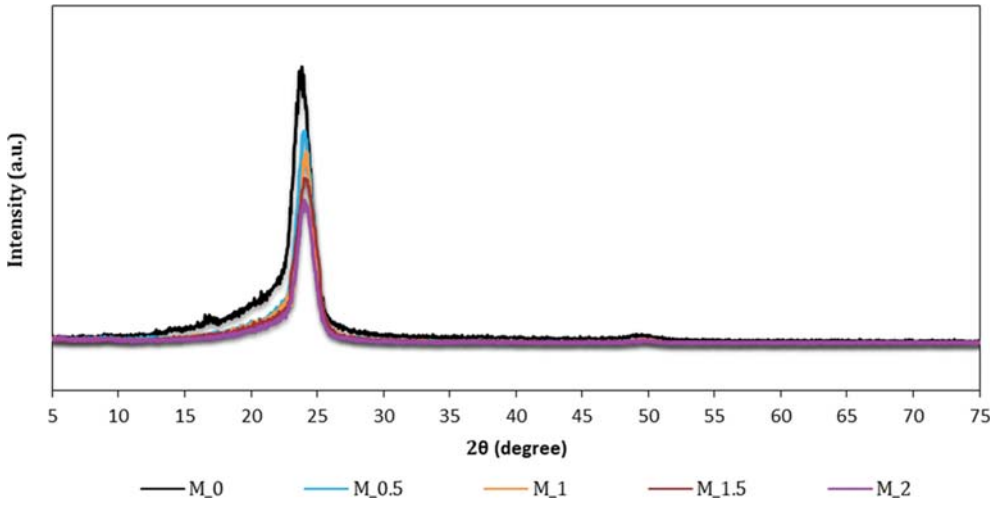

Fig. 3. XRD patterns of the resulting membranes: M_0, M_0.5, M_1, M_1.5 and M_2.

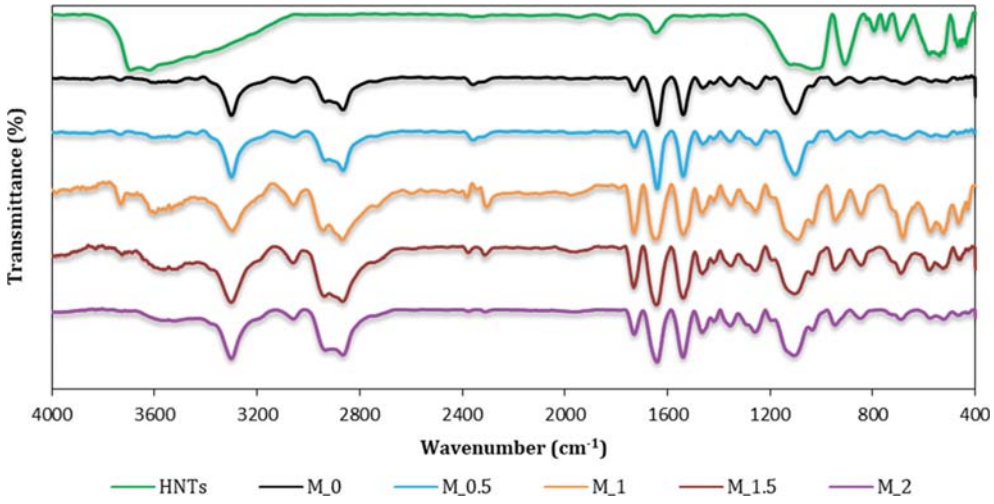

Fig. 4. FT-IR spectra of the HNTs, and the resulting membranes: M_0, M_0.5, M_1, M_1.5, and M_2.

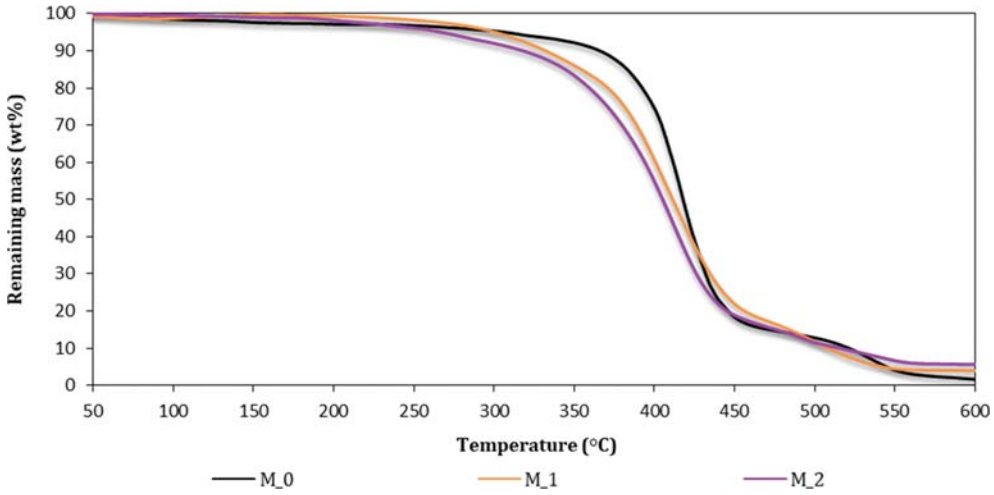

Fig. 5. TGA curves for the resulting membranes: M_0, M_1, and M_2 obtained in air atmosphere.

perpendicular Si-O stretching at 697 cm^{-1}, symmetric stretching of Si-O at 790 cm^{-1}, a double inplane Si-O stretching peaks at 1,035 cm^{-1}, O-H stretching vibration of inner and inner-surface hydroxyl groups at 3,618, and 3,693 cm^{-1}, respectively [35,52]. The related peaks' intensities are enhanced by raising the HNTs content in the MMMs. The FT-IR outcomes are in good compromise with the those of XRD as explained earlier. It means that both analyses indicate that with increasing the HNTs loading, the disconnection of hydrogen bonding among the PA blocks of the Pebax, as well as the reduction of the membranes crystallinities eventuate [28,46,53].

1-4. TGA

To survey the influence of HNTs loading on the thermal stability of the resulting membranes, TGA was conducted for M_0, M_1, and M_2 membranes. Thermal stability of the membranes based on their residual mass (wt%) is demonstrated in Fig. 5. As depicted, thermal mass loss of the membranes takes place in three stages. The first step from 50 to 350 °C for the M_0, is indicative of the residual solvent, as well as the likely adsorbed moisture vaporization. The second thermal degradation step from 350 to 475 °C expresses degradation of the polymer chains, and also evaporation of the bound moisture in the HNTs. The final step starting at 475 °C, represents the carbonization of the degraded Pebax chains. The above-mentioned steps for the HNTs-loaded membranes occur at different temperature ranges [54-56]. The results show that the introduction of the HNTs into the polymer matrix nearly reduces thermal stability of the resultant MMMs in comparison to the neat membrane. This reduction can be ascribed to the higher thermal conductivity of the HNTs compared to the polymer. This makes the MMMs have lower thermal resistance than the pristine membrane. Notably, thermal stability of all the prepared membranes is high enough for experimental tests at typical operating temperatures [57].

2. Gas Permeation Experiment

2-1. HNTs Loading Influence

The effect of the embedded HNTs amount on the gas permeation features of the resulting membranes at a constant pressure of 4 bar is displayed in Fig. 6. As shown, the permeability of both CO_2 and CH_4 gases rose from 76.50 and 3.22 to 101.23 and 5.05 Bar-

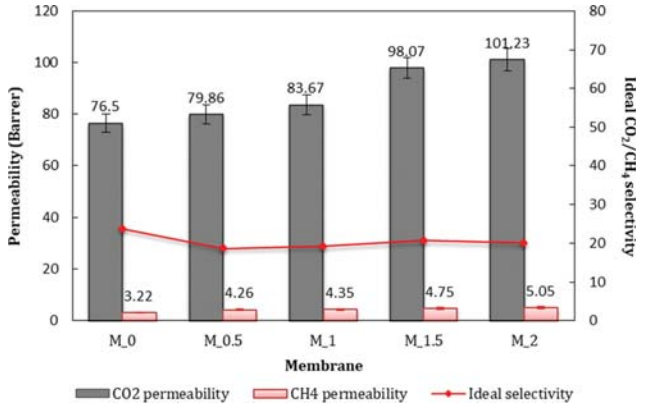

Fig. 6. Influence of HNTs loading on gas permeation features of the resulting membranes at 25 °C and 4 bar.

rer, respectively, when the HNTs loading increased from 0 to 2 wt%, which most likely resulted from the crystallinity decrement of the polymer matrix via the HNTs incorporation. In fact, the embedded HNTs ruptured the interchain hydrogen bonds among the PA blocks, as previously affirmed by the FT-IR and XRD analyses. The crystalline phase of the polymer is normally assumed to be impermeable to the passage of gas species [36,58]. Adding the permeable HNTs into the polymer matrix can also cause higher diffusivity of CO_2 and CH_4 gases, and consequently, their more permeability through the resultant MMMs compared to the pristine membrane. Additionally, the results indicate more CO_2 permeability than CH_4 through all the prepared membranes (see Fig. 6). The main reason for this behavior is the higher CO_2 solubility into the prepared membranes, resulting from its higher condensability compared to CH_4 (T_c of CO_2 is 31.1 °C, while that of CH_4 is −82.3 °C) as well as, its more diffusivity due to its smaller kinetic diameter (kinetic diameter of CO_2 is 3.3 Å, whereas that of CH_4 is 3.8 Å). Also, the PEBAX polar group affinity to CO_2 (which is polar) is more than that to the non-polar gas (CH_4). Thus, its permeability coefficient, which is the multiplication of solubility and diffusivity, is higher than that of CH_4 for all the fabricated membranes. Particularly, for the MMMs, this increment can also result from the higher capacity of HNTs for CO_2 adsorption.

Although permeabilities of both gases through the MMMs are greater than those of the neat membrane, the ideal CO_2/CH_4 selectivity of all the prepared MMMs is lower than that of the pristine membrane. This is likely owing to the more increase of CH_4 permeability through the MMMs compared to that through the pristine membrane. In fact, presence of the non-selective HNTs due to their large lumen diameters in the Pebax matrix causes CH_4 to diffuse more compared with the case when no HNTs within the polymeric matrix of the membrane are present [34,35]. However, the ideal selectivity of the MMMs is enhanced from 18.75 to 20.64 by increasing the HNTs loading from 0.5 to 1.5 wt%. This trend is probably attributed to the greater enhancement of CO_2 permeability than that of CH_4 because of the more considerable affinity of HNTs to CO_2 molecules, resulting from the greater adsorption capability of HNTs for CO_2 molecules than CH_4 ones [59]. As seen in Fig. 6, with increasing the HNTs content more than 1.5 wt%, the

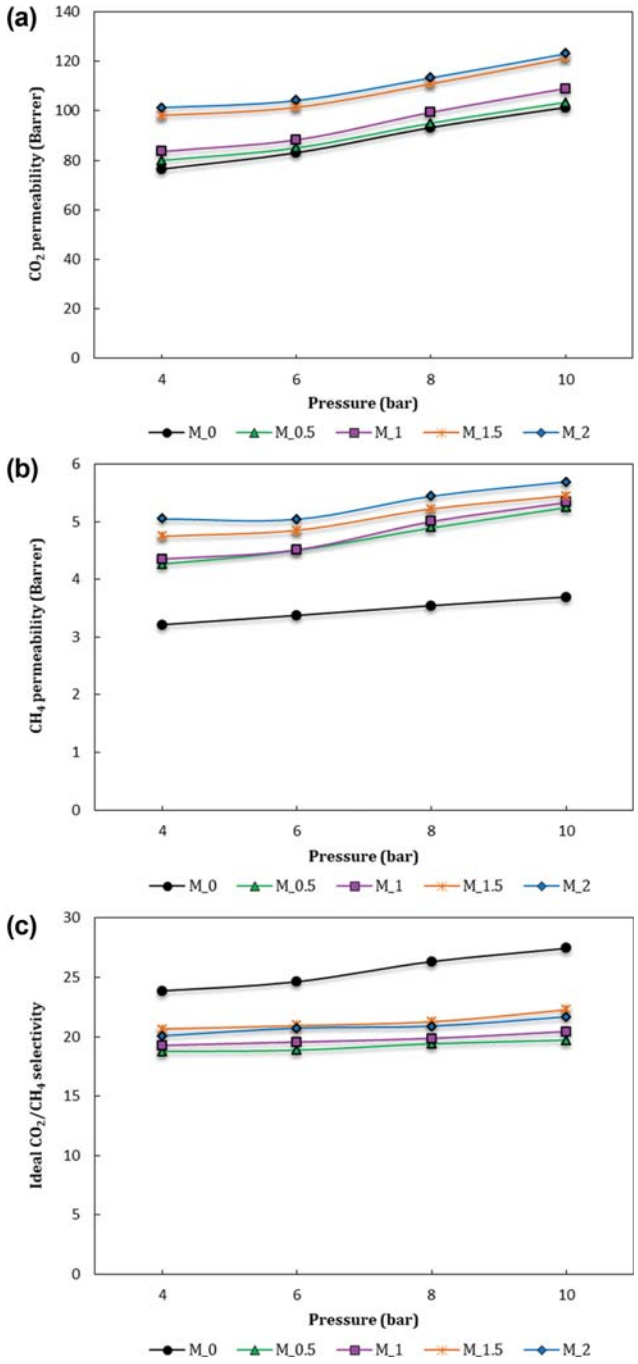

Fig. 7. Influence of feed pressure on (a) CO_2 permeability, (b) CH_4 permeability, and (c) Ideal CO_2/CH_4 selectivity values of the membranes at 25 °C.

ideal selectivity experiences a descending trend because the tendency of HNTs for agglomeration in the polymer matrix increases, and accordingly, CO_2 permeability does not exhibit the previous improvement. Similarly, Hashemifard et al. prepared PEI-based MMMs loaded with HNTs and found that with increasing the nanotubes from 0 to 1 wt%, permeability of both gases increases, while ideal CO_2/CH_4 selectivity firstly increases and then decreases [35].

2-2. Feed Pressure Influence

To observe the influence of enhancing feed pressure on gas sep-

aration efficiency of the fabricated membranes, the gas permeability and ideal selectivity of the neat membrane and the MMMs loaded with various HNTs amounts at diverse pressures (4, 6, 8, and 10 bar) is depicted in Fig. 7. As seen in Fig. 7(a) and (b), by increasing the feed pressure from 4 to 10 bar, both CO_2 and CH_4 permeability increases for all the membranes, resulting from the improved mass transfer driving force and solubility coefficient of the penetrants. For example, for the M_0 and M_2 membranes, CO_2 permeability increases from 76.50 and 101.23 Barrer to 101.31 and 123.21 Barrer, while that of CH_4 increases from 3.22 and 5.05 Barrer to 3.69 and 5.69 Barrer, respectively. However, as seen, CO_2 permeability is enhanced more than that of CH_4. Particularly for the neat membrane (M_0), the higher CO_2 condensability compared to CH_4, as well as its more affinity to the polar ether groups of the Pebax, lead to the greater CO_2 solubility into the membrane. Moreover, as kinetic diameter of CO_2 molecules is smaller than that of CH_4 molecules; they can diffuse quicker at higher pressure [60,61]. For the MMMs, the greater CO_2 permeability enhancement in comparison with that of CH_4 originates from the greater CO_2 adsorption capacity increment of the HNTs. Additionally, the membrane plasticization by CO_2 molecules, enhancing the chain spacing and the chain mobility of the polymer, resulting in the enlarged penetrants diffusion coefficients, can be considered as another reason for this phenomenon [62]. As a result, the rate of permeability enhancement with pressure is sharper for CO_2 than CH_4, and accordingly, the membranes' ideal CO_2/CH_4 selectivity increases with the pressure growth, as in Fig. 7(c). For instance, the ideal selectivity of the M_0 and M_2 membranes increases from 23.79, and 20.05 to 27.42 and 21.65 when the pressure increases from 4 to 10 bar.

3. Comparison of the Obtained Results with those in the Literature and the Robeson's Upper Bound Lines

The results of CO_2/CH_4 separation performance of the optimum membrane synthesized and characterized in the present study and those of other Pebax-based membranes in the previous studies are listed in Table 2 [21,27,49,59,63-65]. As observed, the M_1.5 membrane exhibits CO_2 permeability and ideal CO_2/CH_4 selectivity of 98.07 Barrer, and 20.65, respectively, at 25 °C and 4 bar. In comparison with the other Pebax-based membranes, the optimum MMM obtained in this study (M_1.5) shows nearly favorable separation efficiency.

A standard method to investigate the efficiency of gas separation membranes is the consideration of their permeability-selectivity data points in the Robeson diagrams [15,16]. Until now, researchers have intensively tried to approach the diagram bound lines (Robeson's upper bound lines were presented in 1991 and 2008). Accordingly, in the current study, the fabricated membranes separation characteristics at the pressure of 4 bar were considered in Robeson's diagram (Fig. 8) to be compared with its upper bound lines.

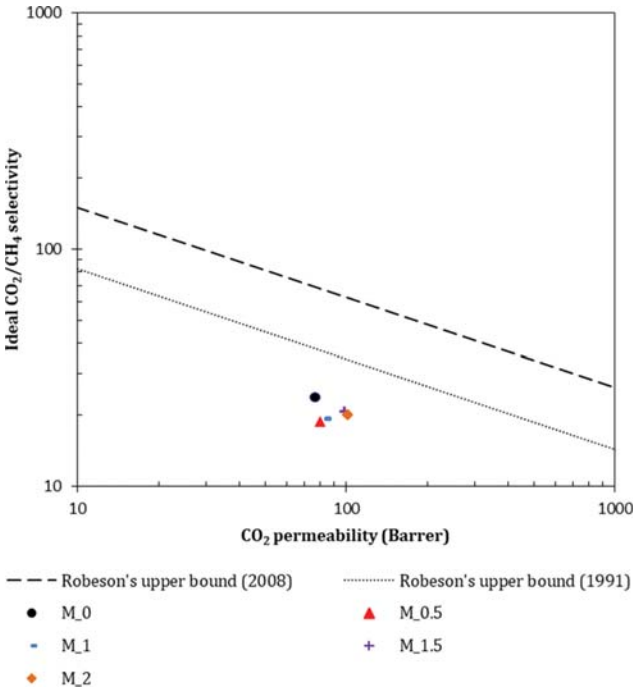

Fig. 8. Comparison of the resulting membranes' efficiencies with the Robeson's upper bound lines for CO_2/CH_4 separation.

As shown in Fig. 8, the data points' positions of the resulting MMMs do not become close to Robeson's upper bound lines compared to the pristine membrane. Thus, although the CO_2 permeability of the membranes is enhanced with increasing the HNTs loading, their ideal selectivity relative to that of the neat Pebax membrane does not considerably alter; therefore, the Pebax-1657/HNTs MMMs cannot be commercialized as candidates for CO_2/CH_4 separation without any surface modification of the HNTs.

Table 2. Comparison of CO_2/CH_4 separation performance of the optimum MMM prepared in this study with those of Pebax-based MMMs in the literature

Filler type	Filler amount (wt%)	Pressure (bar)	Temperature (°C)	P_{CO_2} (Barrer)	α (CO_2/CH_4)	Ref.
ImGO	0.8	4	25	64.0	25.1	[21]
SAPO-34	23	7	35	135.0	20.8	[27]
4A Zeolite	10	5	25	97.0	26.4	[50]
Al_2O_3	8	3	25	159.3	24.7	[59]
Fumed SiO_2	10	8	25	60.1	26.1	[63]
Fe-BTC	30	3	25	148.4	21.9	[64]
ZIF-7	22	3.75	25	111.0	30.0	[65]
HNT	1.5	4	25	98.1	20.6	This study

CONCLUSION

Pebax-1657 was employed as the base polymer for fabricating the pristine and MMMs loaded with different HNTs content (0, 0.5, 1, 1.5, and 2 wt% of the polymer weight). The FESEM analysis confirmed the uniform distribution of the HNTs in the Pebax matrix and defect-free structure as well for nearly all the content. The membrane characterization results via XRD and FT-IR analyses revealed that by raising the HNTs loading, the total crystallinity of the membranes decreases as the intersegment hydrogen bonds connecting the PA blocks are disrupted, and expectedly the both CO_2 and CH_4 gases permeabilities increase. Gas permeation experiments using a pressure-constant setup were carried out to study the influences of various parameters such as the HNTs loadings, and the operating pressure on the CO_2/CH_4 separation features of the fabricated membranes. The obtained outcomes indicated that, under the same conditions, the gases' permeabilities through the MMMs are greater than those through the neat membrane. However, the MMMs exhibit lower ideal selectivity compared to the pristine membrane ascribed to the presence of non-selective nanotubes in their matrices. Additionally, comparing all the prepared MMMs, the 1.5 wt% loaded MMM (M_1.5) shows an optimum CO_2 permeability-ideal CO_2/CH_4 selectivity combination and also the best position in Robeson's diagram.

REFERENCES

1. N. Azizi and M. M. Zarei, *Pet. Sci. Technol.*, **35**, 869 (2017).
2. N. Azizi, T. Mohammadi and R. M. Behbahani, *J. Nat. Gas Sci. Eng.*, **37**, 39 (2017).
3. R. Baker, *Membrane technology and applications*, Wiley, Newark, California, USA (2012).
4. V. Bondar, B. Freeman and I. Pinnau, *J. Polym. Sci. B Polym. Phys.*, **38**, 2051 (2000).
5. N. Azizi, H. R. Mahdavi, M. Isanejad and T. Mohammadi, *J. Polym. Res.*, **24**, 141 (2017).
6. M. Wang, Z. Wang, S. Zhao, J. Wang and S. Wang, *Chin. J. Chem. Eng.*, **25**, 1581 (2017).
7. G. George, N. Bhoria, S. AlHallaq, A. Abdala and V. Mittal, *Sep. Purif. Technol.*, **158**, 333 (2016).
8. X. Ren, J. Ren, H. Li, S. Feng and M. Deng, *Int. J. Greenh. Gas Control*, **8**, 111 (2012).
9. L. Zhao, Y. Chen, B. Wang, C. Sun, S. Chakraborty, K. Ramasubramanian, P. K. Dutta and W. W. Ho, *J. Membr. Sci.*, **498**, 1 (2016).
10. Y. Chen, B. Wang, L. Zhao, P. Dutta and W. W. Ho, *J. Membr. Sci.*, **495**, 415 (2015).
11. M. Di Lorenzo, M. Pyda and B. Wunderlich, *J. Polym. Sci. B Polym. Phys.*, **39**, 1594 (2001).
12. G. R. Hatfield, Y. Guo, W. E. Killinger, R. A. Andrejak and P. M. Roubicek, *Macromolecules*, **26**, 6350 (1993).
13. E. Konyukhova, A. Buzin and Y. K. Godovsky, *Thermochim. Acta*, **391**, 271 (2002).
14. N. Azizi, T. Mohammadi and R. M. Behbahani, *J. Energy Chem.*, **26**, 454 (2017).
15. L. M. Robeson, *J. Membr. Sci.*, **62**, 165 (1991).
16. L. M. Robeson, *J. Membr. Sci.*, **320**, 390 (2008).
17. S. Feng, J. Ren, K. Hua, H. Li, X. Ren and M. Deng, *Sep. Purif. Technol.*, **116**, 25 (2013).
18. C. Karthikeyan, S. Nunes, L. Prado, M. Ponce, H. Silva, B. Ruffmann and K. Schulte, *J. Membr. Sci.*, **254**, 139 (2005).
19. L. Wang, Y. Li, S. Li, P. Ji and C. Jiang, *J. Energy Chem.*, **23**, 717 (2014).
20. A. Khoshkharam, N. Azizi, R. M. Behbahani and M. A. Ghayyem, *Pet. Sci. Technol.*, **35**, 667 (2017).
21. Y. Dai, X. Ruan, Z. Yan, K. Yang, M. Yu, H. Li, W. Zhao and G. He, *Sep. Purif. Technol.*, **166**, 171 (2016).
22. A. Jomekian, R. M. Behbahani, T. Mohammadi and A. Kargari, *J. Nat. Gas Sci. Eng.*, **31**, 562 (2016).
23. L.-E. José Cirilo Ignacio, L. Ant, S. Karl and B. Emilio, *Open J. Polym. Chem.*, **2012**, 63 (2012).
24. N. Azizi, M. Arzani, H. R. Mahdavi and T. Mohammadi, *Korean J. Chem. Eng.*, **34**, 2459 (2017).
25. N. Azizi, M. Isanejad, T. Mohammadi and R. M. Behbahani, *Front Chem. Sci. Eng.*, **13**, 517 (2019).
26. L. Xu, L. Xiang, C. Wang, J. Yu, L. Zhang and Y. Pan, *Chin. J. Chem. Eng.*, **25**, 882 (2017).
27. D. Zhao, J. Ren, H. Li, K. Hua and M. Deng, *J. Energy Chem.*, **23**, 227 (2014).
28. D. Zhao, J. Ren, H. Li, X. Li and M. Deng, *J. Membr. Sci.*, **467**, 41 (2014).
29. M. H. Jazebizadeh and S. Khazraei, *Silicon*, **9**, 775 (2017).
30. R. S. Murali, A. F. Ismail, M. A. Rahman and S. Sridhar, *Sep. Purif. Technol.*, **129**, 1 (2014).
31. V. Nafisi and M.-B. Hägg, *J. Membr. Sci.*, **459**, 244 (2014).
32. A. Ehsani and M. Pakizeh, *J. Taiwan Inst. Chem. Eng.*, **66**, 414 (2016).
33. R. Surya Murali, M. Padaki, T. Matsuura, M. Abdullah and A. Ismail, *Sep. Purif. Technol.*, **132**, 187 (2014).
34. A. Ismail, S. Hashemifard and T. Matsuura, *J. Membr. Sci.*, **379**, 378 (2011).
35. S. Hashemifard, A. Ismail and T. Matsuura, *J. Colloid Interface Sci.*, **359**, 359 (2011).
36. N. Azizi, T. Mohammadi and R. Mosayebi Behbahani, *Chem. Eng. Res. Des.*, **117**, 177 (2017).
37. M. Isanejad, N. Azizi and T. Mohammadi, *J. Appl. Polym. Sci.*, **134**, 44531 (2017).
38. L. Xiang, Y. Pan, G. Zeng, J. Jiang, J. Chen and C. Wang, *J. Membr. Sci.*, **500**, 66 (2016).
39. T. Fan, W. Xie, X. Ji, C. Liu, X. Feng and X. Lu, *Chin. J. Chem. Eng.*, **24**, 1513 (2016).
40. S. Wang, Y. Liu, S. Huang, H. Wu, Y. Li, Z. Tian and Z. Jiang, *J. Membr. Sci.*, **460**, 62 (2014).
41. S. Stern, *J. Polym. Sci. Part A-2: Polym. Phys.*, **6**, 1933 (1968).
42. J. H. Kim and Y. M. Lee, *J. Membr. Sci.*, **193**, 209 (2001).
43. Z. Farashi, N. Azizi and R. Homayoon, *Pet. Sci. Technol.*, **37**, 2412 (2019).
44. A. F. Ismail, K. C. Khulbe and T. Matsuura, *Gas separation membranes: Polymeric and inorganic*, Springer, Switzerland (2015).
45. Y. Wang, J. Ren and M. Deng, *Sep. Purif. Technol.*, **77**, 46 (2011).
46. R. Surya Murali, S. Sridhar, T. Sankarshana and Y. Ravikumar, *Ind. Eng. Chem. Res.*, **49**, 6530 (2010).
47. Y. Yampolskii and B. Freeman, *Membrane gas separation*, Wiley

Online Library (2010).
48. A. Ghadimi, M. Amirilargani, T. Mohammadi, N. Kasiri and B. Sadatnia, *J. Membr. Sci.*, **458**, 14 (2014).
49. M. Ariazadeh, Z. Farashi, N. Azizi and M. Khajouei, *Korean J. Chem. Eng.*, **37**, 295 (2020).
50. R. Surya Murali, A. F. Ismail, M. A. Rahman and S. Sridhar, *Sep. Purif. Technol.*, **129**, 1 (2014).
51. H. Rabiee, S. Meshkat Alsadat, M. Soltanieh, S. A. Mousavi and A. Ghadimi, *J. Ind. Eng. Chem.*, **27**, 223 (2015).
52. M. Mansour Sharifloo, A. Ghaee, E. Salimi, B. Sadatnia and Z. Mansourpour, *Int. J. Polymer. Mater. Polymer. Biomater.*, **68**, 762 (2019).
53. B. Yu, H. Cong, Z. Li, J. Tang and X. S. Zhao, *J. Appl. Polym. Sci.*, **130**, 2867 (2013).
54. N. A. H. M. Nordin, S. M. Racha, T. Matsuura, N. Misdan, N. A. A. Sani, A. F. Ismail and A. Mustafa, *RSC Adv.*, **5**, 43110 (2015).
55. N. A. H. M. Nordin, A. F. Ismail, A. Mustafa, R. S. Murali and T. Matsuura, *RSC Adv.*, **5**, 30206 (2015).
56. F. Dorosti, M. Omidkhah and R. Abedini, *J. Nat. Gas Sci. Eng.*, **25**, 88 (2015).
57. S. Meshkat, S. Kaliaguine and D. Rodrigue, *Sep. Purif. Technol.*, **200**, 177 (2018).
58. A. Ghadimi, T. Mohammadi and N. Kasiri, *Int. J. Hydrogen Energy*, **40**, 9723 (2015).
59. Z. Farashi, S. Azizi, M. R.-D. Arzhandi, Z. Noroozi and N. Azizi, *J. Nat. Gas Sci. Eng.*, **72**, 103019 (2019).
60. M. Sadeghi, M. M. Talakesh, B. Ghalei and M. Shafiei, *J. Membr. Sci.*, **427**, 21 (2013).
61. M. M. Rahman, V. Filiz, S. Shishatskiy, C. Abetz, S. Neumann, S. Bolmer, M. M. Khan and V. Abetz, *J. Membr. Sci.*, **437**, 286 (2013).
62. E. C. *Suloff, Sorption behavior of an aliphatic series of aldehydes in the presence of poly (ethylene terephthalate) blends containing aldehyde scavenging agents*, Virginia Tech, Blacksburg, Virginia (2002).
63. Z. Aghaei, L. Naji, V. H. Asl, G. Khanbabaei and F. Dezhagah, *Sep. Purif. Technol.*, **199**, 47 (2018).
64. F. Dorosti and A. Alizadehdakhel, *Chem. Eng. Res. Des.*, **136**, 119 (2018).
65. T. Li, Y. Pan, K.-V. Peinemann and Z. Lai, *J. Membr. Sci.*, **425**, 235 (2013).